Simultaneous magnetic and chemical imaging of Nd-Fe-B thin films by means of XMCD-PEEM technique

R. Goto[1,*], S. Okamoto[1, 2], T. Ohkochi[3], N. Kikuchi[1], O. Kitakami[1], and T. Nakamura[2, 3]

[1] Institute of Multidisciplinary Research for Advanced Materials (IMRAM), Tohoku University, *2-1-1 Katahira, Aoba-ku, Sendai 980-8577, Japan*

[2] Elements Strategy Initiative Center for Magnetic Materials (ESICMM), National Institute for Materials Science, *1-2-1 Sengen, Tsukuba, Ibaraki 305-0047, Japan*

[3] Japan Synchrotron Radiation Research Institute/SPring-8, *1-1-1, Kouto, Sayo-cho, Sayo-gun, Hyogo 679-5198, Japan*

The coercivity mechanism of Nd-Fe-B thin film samples with and without Nd deposition was investigated by simultaneous chemical and magnetic imaging by means of X-ray magnetic circular dichroism-photoemission electron microscopy. The two Nd-Fe-B thin film samples exhibited almost the same surface morphology and magnetic domain patterns, but their coercive fields were quite different, being 0.98 T for the sample with Nd deposition and 0.55 T for sample without Nd deposition. The chemical distribution of Nd revealed that Nd aggregates with the average size of 130 nm exist, and the density in the Nd-deposited sample is much higher than that in the not deposited one. A comparison of the magnetic and chemical contrast images implied that the Nd aggregates act as domain wall pinning sites, indicating that the large coercivity difference in the Nd-Fe-B thin films would be attributable to the different density of wall pinning sites.

Key words: Neodymium-Iron-Boron magnets, thin films, magnetic reversal, X-ray magnetic circular dichroism, photoelectron emission microscopy

1. Introduction

Nd-Fe-B magnets are a key material for high efficiency electric generators and motors. For these applications, numerous attempts have been made to enhance the coercivity while maintaining high saturation magnetization. Although heavy rare earth (RE) elements such as Dy or Tb are usually added to increase the coercivity of Nd-Fe-B magnets, these RE elements degrade their saturation magnetization due to antiferromagnetic coupling between 3d and 4f magnetic moments. Moreover, the availability and price of the heavy RE elements are currently serious resource problems. Recently, the coercivity $\mu_0 H_c$ of Nd-Fe-B sintered magnets has been successfully enhanced to about 2 T even without addition of heavy RE elements by various methods such as refinement of the constituent crystal grains of the $Nd_2Fe_{14}B$ phase [1] and/or grain boundary diffusion of RE elements to restore magnetic anisotropy near the grain boundaries or to suppress intergranular exchange coupling [2, 3]. However, the $\mu_0 H_c$ obtained by these techniques remains much smaller than the anisotropy field of $\mu_0 H_k = 7.5$ T [4].

The large discrepancy between the $\mu_0 H_c$ and $\mu_0 H_k$ observed in a wide variety of permanent magnets, which is known as Brown's paradox [5], is the subject of a long-standing debate in magnetics. To solve this problem, a detailed analysis of the magnetization reversal process is indispensable. So far it is widely accepted that nucleation of reversed domains dominates the magnetization reversal in Nd-Fe-B magnets, judging from the initial and minor magnetization curve behaviors [6]. On the other hand, the angular dependence and *c*-axis dispersion dependence of $\mu_0 H_c$ [7, 8] strongly suggest that domain wall depinning is the dominant process in Nd-Fe-B magnets.

Recently, we proposed a new approach to examine the magnetization reversal process [9]. At a finite temperature, magnetization reversal proceeds under the influence of thermal activation, which enables the magnetization to overcome a finite energy barrier separating local energy minima. The energy barrier is a function of a magnetic field H, and its function form depends on the magnetization reversal process. For example, the energy barrier is a quadratic function of H for coherent rotation and/or nucleation [10] and a linear function of H for weak pinning of a domain wall [11]. The energy barrier function can be determined experimentally by analysis of magnetic viscosity measurements. We applied this type of analysis to two kinds of (001) oriented Nd-Fe-B thin film samples with and without a Nd overlayer which is preferentially diffused along the Nd-Fe-B grain boundaries during the deposition [9]. In spite of the large difference in their coercivities, both of their barriers were found to be linear functions of H, suggesting that weak domain wall pinning is dominant in both samples. It should be stressed here that the above two Nd-Fe-B thin film samples have almost the same structures, such as *c*-axis orientation, grain size, and so on. In order to understand the reason for the large coercivity

difference mentioned above, simultaneous magnetic and chemical distribution imaging were performed on the two Nd-Fe-B film samples by means of X-ray magnetic circular dichroism-photoemission electron microscopy (XMCD-PEEM).

2. Experiments

Nd-Fe-B thin films examined in the present study are grown on MgO (001) substrates with the layer structure of MgO/Mo(30 nm)/Nd(0.25 nm)/Nd-Fe-B(50 nm)/Nd(t_{Nd} = 0, 1 nm)/Mo(10 nm). For brevity, the Nd-Fe-B film samples with and without a Nd deposition are denoted as Nd-Fe-B/Nd and Nd-Fe-B, respectively. The composition of the Nd-Fe-B layer is adjusted to $Nd_{12.8}Fe_{78.7}B_{8.5}$ in at% by controlling the sputtering rates of Nd, Fe, and B. The substrate is kept at T_s = 500°C during deposition of both Nd-Fe-B and Nd. The detailed sample fabrication conditions and magnetic and structural characterization methods are described elsewhere [9]. Since both Nd-Fe-B/Nd and Nd-Fe-B are prepared under the same condition, they have the same crystal structure with good *c*-axis orientation. The surface morphologies and magnetic domain structures were observed by atomic force microscopy (AFM) and magnetic force microscopy (MFM), respectively. X-ray magnetic circular dichroism-photoemission electron microscopy (XMCD-PEEM) was performed with Nd $M_{4,5}$ and Fe $L_{2,3}$ edges at the BL25SU beamline of SPring-8. Soft X-rays were incident on the sample at 30 degree with respect to the sample plane, enabling us to detect perpendicular component of the magnetizations. Prior to the XMCD-PEEM experiment, the Mo capping layers were etched *ex situ* down to about 5 nm considering the very short probing depth of PEEM. The samples were observed at room temperature without application of a magnetic field.

3. Results and Discussions

Figures 1(a) and 1(b) show the perpendicular magnetization curves of Nd-Fe-B and Nd-Fe-B/Nd, respectively. While they both exhibit high remanence ratios, their coercive fields are quite different, being $\mu_0 H_c$ = 0.55 T for Nd-Fe-B and 0.98 T for Nd-Fe-B/Nd. According to the AFM images in Figs. 1(c) and 1(d), both samples have a partially-connected island structure with the mean size of 100±50 nm. Figures 1(e) and 1(f) show the MFM images of thermally demagnetized Nd-Fe-B and Nd-Fe-B/Nd, respectively. Their domain structures are very similar with the average size of 200 nm. This is roughly two times larger than the grain size in Figs.1 (c) and 1(d), indicating that each Nd-Fe-B grain is more or less exchange-coupled to neighboring grains. In spite of the very similar micro- and domain-structures, the Nd-Fe-B with and without Nd deposition exhibit quite

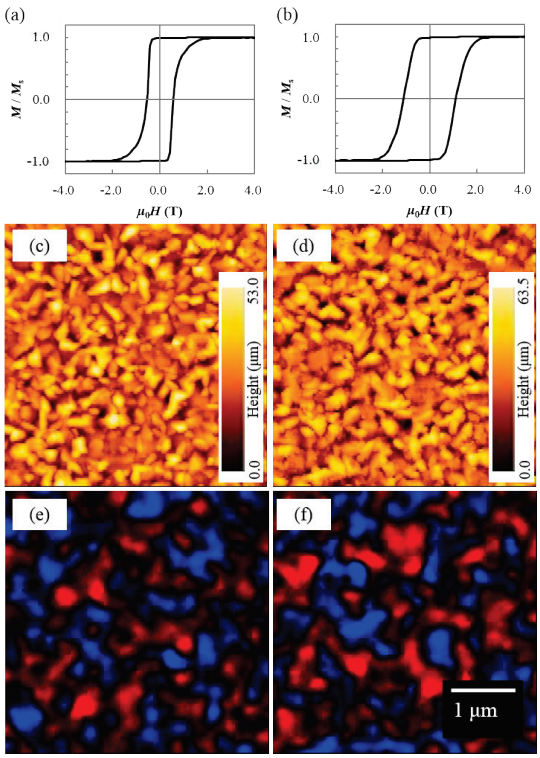

Fig. 1 (a) and (b) perpendicular magnetization curves, (c) and (d) AFM images, and (e) and (f) MFM images of thermal demagnetization states. (a), (c), and (e) show Nd-Fe-B, and (b), (d), and (f) show Nd-Fe-B/Nd.

different coercivities.

In order to explore the reason for the difference, we performed simultaneous chemical and magnetic imaging by means of XMCD-PEEM. Figure 2 shows the X-ray absorption spectra (XAS) of the Nd-Fe-B obtained at the Fe $L_{2,3}$ and Nd $M_{4,5}$ edges. In addition to the clear Fe and Nd absorption edges, a small shoulder is observed at the slightly higher energy side near the Fe L_3 edge owing to oxidation of Fe. This oxidation may be caused by partial over-etching of the Mo capping layer. We believe this small amount of oxidation does not affect the following discussion.

Figures 3(a) and 3(b) show the chemical contrast maps of Nd for Nd-Fe-B and Nd-Fe-B/Nd, respectively,

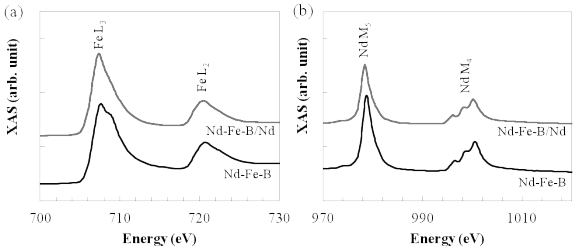

Fig. 2 XAS spectra for (a) Fe $L_{2,3}$ and (b) Nd $M_{4,5}$ edges of Nd-Fe-B and Nd-FeB/Nd.

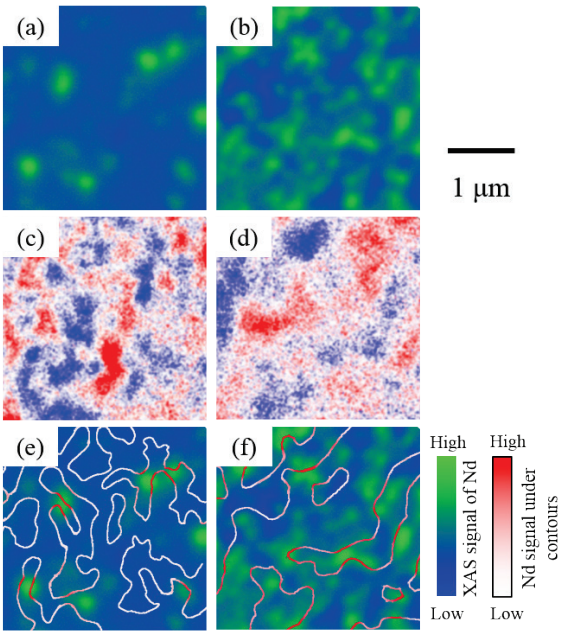

Fig. 3 (a) and (b) chemical contrast images of Nd, (c) and (d) magnetic contrast images, and (e) and (f) contours of magnetic contrast shown in (c) and (d) overlapped with Nd chemical images. The red-colored contrast of contours corresponds to the Nd content under themselves. (a), (c), and (e) show Nd-Fe-B, and (b), (e), and (f) show Nd-Fe-B/Nd.

which were displayed as the spatial distributions of the photoemission intensities at the Nd M_5-edge (978.5 eV) normalized to those at a pre-absorption-edge (972.0 eV). Since Nd is one of the main constituents of the samples, Nd is distributed over the whole area of the samples, as indicated by the blue-colored areas in Figs. 3(a) and 3(b). In addition to this uniform Nd distribution, many tiny Nd-rich aggregates with the size of 130 nm can be clearly observed as indicated by green areas in the same figures. Obviously, the density of the Nd aggregates in Nd-Fe-B/Nd is much higher than that in Nd-Fe-B. According to cross-sectional transmission electron microscopy (TEM) observation of the Nd-Fe-B film prepared under the same conditions, Nd aggregates exist laterally beside the Nd-Fe-B particles on the Mo buffer layer [12]. Figures 3(c) and 3(d) show XMCD-PEEM images of Nd-Fe-B and Nd-Fe-B/Nd, respectively, which were taken to be the XMCD amplitude defined as the difference of XMCD intensity between the Fe L_3 edge (707.6 eV) and Fe L_2 edge (720.8 eV) to highlight the very weak XMCD contrast. In spite of this data processing, the XMCD contrast is still very weak, probably due to the presence of the Mo capping layer. However, XMCD contrasts reflecting the magnetic domain states can be clearly noted, and the patterns are similar to the MFM images in Figs. 1(e) and 1(f). The average domain width of Nd-Fe-B in fig. 3(c) is about 200 nm, being comparable with the value from MFM images in Fig. 1(e). For Nd-Fe-B/Nd, however, the domain width roughly reaches 400 nm, which is about 2 times larger than that from MFM in Fig. 1(f). This discrepancy is probably brought about by weak magnetic contrast in the XMCD measurements. The contours of these XMCD contrasts are overlaid on the chemical mapping of Nd in Figs. 3(e) and 3(f). Note that the magnetic contours which correspond to domain walls partially run across Nd aggregates as indicated by the red-colored portions on the contours. It suggests that Nd-rich aggregates act as pinning sites of magnetic domain walls. This tendency is more obvious in the Nd-Fe-B/Nd sample shown in Fig. 3(f). Each magnetic contour overlaps multiple Nd aggregates, and in some cases lies along the aggregates. The above observation implies that Nd aggregates act as pinning sites of magnetic domain walls. When a magnetic domain wall is pinned at multiple defects, Nd aggregates in this study, the effective pinning force in the two-dimensional system as in the present study may be proportional to the density of defects [13] if the so-called weak pinning process is dominant [14]. Thus based on the present experimental results, we at present consider that the larger coercivity for Nd-Fe-B/Nd is due to higher density of pinning sites, in this case Nd aggregates. This conclusion is qualitatively consistent with our previous report, in which we found that domain wall pinning was dominant for both Nd-Fe-B and the Nd-Fe-B/Nd samples [9].

4. Conclusion

To discuss the origin of the different coercive fields of Nd-Fe-B thin film samples with and without Nd deposition, simultaneous observations of magnetic and chemical contrast images were carried out by the XMCD-PEEM technique. These two Nd-Fe-B films exhibit almost the same surface morphologies and magnetic domain patterns, but their coercive fields are quite different. From the Nd chemical contrast imaging, it was found that a large number of Nd aggregates with the average size of 130 nm exist, and the density of the Nd aggregates for the Nd deposited sample is much higher than that for not deposited one. Although the XMCD contrasts of these thin film samples were very weak, patterns similar to the MFM images were obtained. A comparison of the chemical and magnetic contrast images implied that the Nd aggregates act as wall pinning sites. This result indicates that the large difference in coercive fields of the Nd-Fe-B thin films with and without Nd deposition is attributable to the different density of wall pinning sites.

Acknowledgements This work was partially supported by the Elements Strategy Initiative Center for

Magnetic Materials from MEXT, the Management Expenses Grants for National Universities Corporations from MEXT, and JSPS KAKENHI Grant Number 24360261. The XMCD measurements were performed with the approval of the Japan Synchrotron Radiation Research Institute (JASRI) (Proposal No. 2014B1272).

References

1) Y. Une and M. Sagawa: *J. Japan Inst. Met.* **76**, 12 (2012).
2) H. Nakamura, K. Hirota, T. Ohashi and T. Minowa: *J. Phys. D. Appl. Phys.* **44** ,064003 (2011).
3) H. Sepehri-Amin, T. Ohkubo and K. Hono: *Acta Mater.* **61** ,1982 (2013).
4) R. Grössinger, X.K. Sun, R. Eibler, K.H.J. Buschow and H.R. Kirchmayr: *J. Magn. Magn. Mater.* **58**, 55 (1986).
5) W.F. Brown, *Rev. Mod. Phys.* **17**, 15 (1945).
6) R. Skomski and J. M. D. Coey: Permanent Magnetism, p.175 (Institute of Physics Publishing, Bristol and Phyiladelphia, 1981).
7) F. Cebollada, M. Rossignol, D. Givord, V. Villas-Boas and J. González: *Phys. Rev. B* **52**, 13511 (1995).
8) Y. Matsuura, J. Hoshijima, R. Ishii, *J. Magn. Magn. Mater.* **336**, 88 (2013).
9) R. Goto, S. Okamoto, N. Kikuchi and O. Kitakami: *J. Appl. Phys.* **117**, 17B514 (2015).
10) E.C. Stoner and E.P. Wohlfarth: *Philos. Trans. R. Soc. A Math. Phys. Eng. Sci.* **240**, 599 (1948).
11) P. Gaunt: *J. Appl. Phys.* **59**, 4129 (1986).
12) R. Goto, S. Okamoto, N. Kikuchi and O. Kitakami: in preparation for submission
13) See, for example, the very simple and classical Neel model on domain wall pinning. (e.g. A. H. Morrish: The Physical Principles of Magnetism (Wiley-IEEE Press, 2001)).
14) According to our previous analysis on magnetic viscosity measurements, the functional form of the energy barrier suggests the weak pinning/depinning process in conventional NdFeB magnets.

Present address
*Santoku Corporation, 4-14-34 Fukaekitamachi, Higashinada-ku, Kobe, Hyogo 658-0013, Japan

Received Sep. 25, 2015; Revised Jan. 29, 2016; Accepted Apr. 11, 2016